BDCM Sensorless Control for Twelve-Step Square-Wave PWM

Hung-Chi Chen
*Department of Electrical Engineering
National Chiao Tung University,
Taiwan.
hcchen@cn.nctu.edu.tw

*Chih-Kai Huang
Energy and Environment Laboratories,
Industrial Technology Research
Institution, Taiwan.

Tzu-Yang Tsai
*Department of Electrical Engineering
National Chiao Tung University,
Taiwan.

Abstract **--** After studying the development of BDCM sensorless control with six-step square-wave PWM (SWPWM) and six-step back-EMF detecting scheme (BEDS), the BDCM sensorless control with twelve-step SWPWM and twelve-step BEDS had been proposed and implemented in this paper. The proposed twelve-step BEDS generates the twelve commutation instants from six back-EMF zero-crossings during each cycle where the six-step BEDS generates the six commutation instants from six back-EMF zero-crossings. Since the analysis of six-step BEDS is helpful to develop the twelve-step BEDS, this paper studies the six-step SWPWM and six-step BEDS first and explains why some specific six-step SWPWM type is always used in the six-step BDCM sensorless control. Then, we obtain the specific twelve-step SWPWM types and develop the proposed twelve-step BEDS. From the simulated and experimental results, BDCM sensorless control with twelve-step SWPWM shows less current harmonics than that with six-step SWPWM.

***Index Terms*—sensorless control, BDCM, twelve-step PWM.**

I. INTRODUCTION

In the normal operations of BDCMs, the discrete rotor positions should be monitored by the mounted position sensors in order to yield adequate current commutations. However, in refrigerant system, the temperature in the hermetic compressors is usually more than $90°C$ which would result in the failures of hall position sensors. It follows that the position sensorless control becomes important for the applications of BDCMs to the inverter-fed refrigerant systems.

In BDCMs, the back-EMFs represent the induced voltages in the stator windings due to the rotation of permanent-magnet rotor. It means that the discrete rotor positions can be obtained from the back-EMF zero-crossings. However, in a voltage source inverter, sensing back-EMF zero-crossings from the motor terminal voltages is not always available. The availability is highly dependent on the used pulse-width-modulation (PWM) patterns [1-2].

Six-step square-wave PWMs (six-step SWPWMs) with 120° conduction are often used in the sensorless BDCM control for that the floating terminal voltage can be represented in terms of the BDCM back-EMFs and the zero-crossings of back-EMF are available. As plotted in Fig. 1, the back-EMF detecting scheme (BEDS) is used to obtain the commutation signal H from the terminal voltages and then, generate the estimated speed ω_r and the six gate signals. From the literatures, the six-step SWPWMs which had used in the BDCM sensorless control can be divided into four types [3-4]: fully upper PWM (FUPWM) [2, 4-6], fully lower PWM (FLPWM) [7], alternatively leading PWM (ALeadPWM) [8] and alternatively lagging PWM (ALagPWM) [9-10].

Many BEDSs had been proposed in the literatures and can be divided into two groups. One group is based on the frequency responses of passive filters, including low-pass filters and and-pass filters [2,4-6,11-12]. The commutation signal H is obtained from the compared results of three filtered signals of terminal voltages and a pseudo-neutral signal. However, due to the capacitors in these passive filters, the yielded phase delay of commutation signal H varies with the BDCM speed and the position-dependent load torque [4], and thus, the BEDSs in this group are not suitable in the variable-speed sensorless applications.

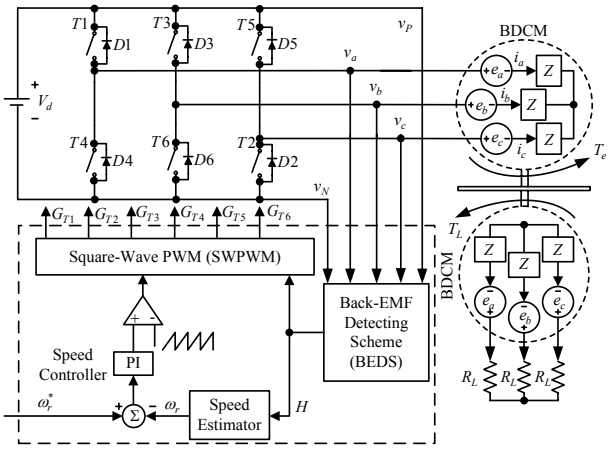

Fig. 1. sensorless BDCM control with back-EMF detecting scheme.

To overcome the phase-delay problem resulting from the passive filters, the other group including two types of phase-delay-free BEDSs had been proposed where one uses A/D converters [13-14] and the other uses comparators [9-10], respectively. The former type of phase-delay-free BEDS is able to obtain commutation signal H with all six-step SWPWM because the terminal voltage had been monitored by the A/D converter.

In the latter type, the commutation signal H is obtained by separating the back-EMF zero-crossings from the comparisons between the three terminal voltages and the half dc-link voltage. However, various six-step SWPWMs may lead to various terminal voltage waveforms and various comparisons. From the study, removing the ALagPWM transitions from the comparisons is easier than removing

FUPWM, FLPWM and ALeadPWM. Unlike the former type of BEDS, only ALagPWM can be used with the comparator-based phase-delay-free BEDS in the sensorless BDCM control [4].

It is noted that more and more sinusoidal-wave back-EMF BDCMs are used to replace for sinusoidal-wave back-EMF BDCMs with square-wave current in order to simply the supply of BDCMs. Due to twelve commutations in twelve-step square-wave modulation (i.e. 150° SWM), twelve-step square-wave nodulation (SWM) possesses less voltage harmonics than six-step SWM [15-16]. Recently, the use of twelve-step SWM in the fix-speed BDCM sensorless control [16-17] and the use of the twelve-step SWPWM in a variable-speed BDCM sensorless control are increasing [18].

In this paper, a comparator-based phase-delay-free BEDS for twelve-step SWPWM (named twelve-step BEDS) had been proposed and implemented. First, all twelve-step SWPWM types are studied in order to find the preferred types where the resulting SWPWM transition in comparisons can be removed easily. Then, the comparator-based BEDS for six-step SWPWM is modified to become the one for twelve-step SWPWM. From the simulated and experimental results implemented in MCU-based environment, the proposed BEDS works normally and the yielded harmonics of the used twelve-step SWPWM type-00110_00110 is better than those of ALagPWM (i.e. six-step SWPWM type 01_01).

II. SIX-STEP BEDS

In this section, all defined six-step SWPWM types are studied in order to find those possessing linear modulation (i.e. named linear SWPWM types). Then, from the ease of removing PWM transitions in the comparisons, we can obtain the preferred type for comparator-based phase-delay-free BEDS (i.e. named sensorless SWPWM types). These procedures would help to develop the twelve-step BEDS in the next section.

A. Type Definition for Six-Step SWPWM

In the common six-step SWPWM, each switch conducts for 120° and there are six commutations in each periodic cycle. The available six conduction patterns are plotted in Fig. 2 where only two switches conduct at any instant. It means that there is always a floating inverter leg during each $\pi/3$ period and an equivalent dead-time (or commonly called blanking-time) exists between the two gate signals at the same leg, which avoids the occurrence of short of dc voltage.

From Fig. 2, it is clear that the gate signals G_{T1}, G_{T3}, and G_{T5} of the upper switch is decided by two conduction states U_1, U_2 and the other are related to the states L_1, L_2. It follows that there are total four freedoms involved in the define six-step SWPWM. In order to apply SWPWM to adjust the output voltage, the conduction state in each pattern may be either continuous "on" or discontinuous "on" (i.e. PWM "on") with duty ratio D. Consequently, there are $2^4 = 16$ possible types in six-step SWPWM. As shown in Fig .2, the gate signals of six-step SWPWM type defined as type-$U_1U_2\_L_1L_2$ are

$$G_{Tx} = \begin{cases} \text{Continuous "on"}, & \text{when } U_m = 0 \text{ or } L_n = 0 \\ \text{PWM "on" with duty ratio } D, & \text{when } U_m = 1 \text{ or } L_n = 1 \end{cases} \quad m,n = 1,2 \tag{1}$$

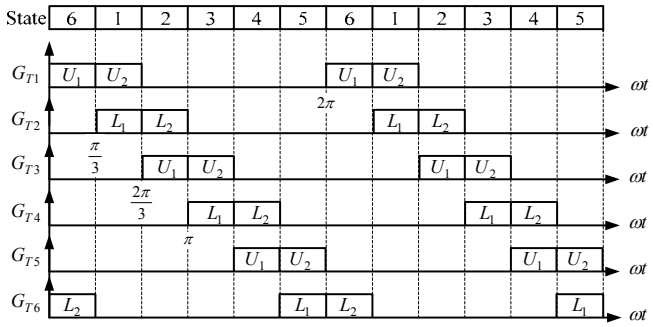

Fig. 2. Type definition of gate signals of six-step SWPWM.

B. Linear Six-Step SWPWM Types

All gate signals for six-step SWPWM type-01_01 and the inverter output voltages are plotted in Fig. 3. Due to $U_1 = L_1 = 0$ and $U_2 = L_2 = 1$ for type-01_01, we can find that each gate signal holds the turn-on level at the first $\pi/3$ period, then alternates periodically for the next $\pi/3$ period, and it blocks at the remaining period. From (1), it is noted that the common six-step SWM can be seen as type-00_00 where its gate signals are always continuous "on" during the conducting period.

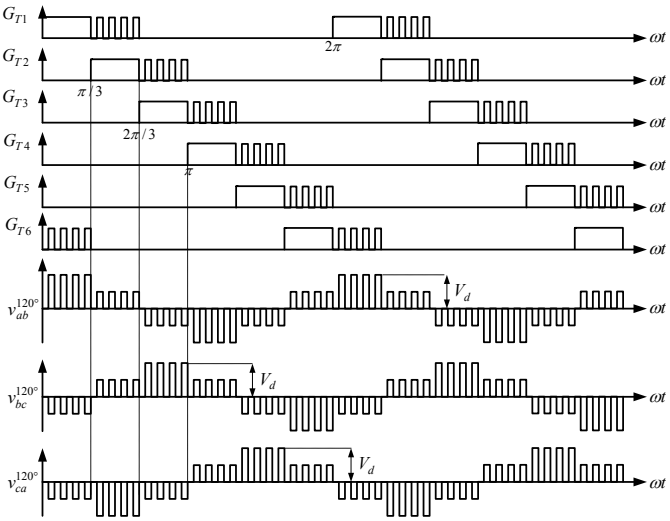

Fig. 3. Illustrated waveforms for type-01_01.

Therefore, FUPWM, FLPWM, ALagPWM and ALeadPWM listed in [4] can be represented as type 11_00, 00_11, 01_01 and 10_10, respectively. The output voltage $v_{ab}^{1\bar{2}0^\circ}$ plotted in Fig. 3 can be expressed in Fourier series as [15]:

$$v_{ab}^{120^\circ}(t)=\sum_{h=1}^{\infty}[\frac{4}{h\pi}DV_d\sin^2(\frac{h\pi}{2})\cos^2(\frac{h\pi}{6})\sin h(2\pi f_1 t+\frac{\pi}{3})] \qquad (2)$$

where f_1 is the fundamental frequency in *Hz*. Due to half-wave symmetry and identified phase displacement $2\pi/3$ between each two leg voltages, all the even and triple harmonics (3, 9, 15 ...) in $v_{ab}^{120^\circ}$ are zeros.

Obviously, the fundamental output voltage of six-step SWPWM type 01_01 can be linearly controlled from near zero to its maximum value $3V_d/\pi$ by adjusting the duty ratio *D*. However, not all six-step SWPWM types define in (1) possess the same linear characteristics. After studying the fundamental voltages of all types, we find that type-00_11, 01_01, 01_11, 10_10, 10_11, 11_00, 11_01, 11_10 and 11_11 could generate linear fundamental output voltages from zero to maximum value $3V_d/\pi$, but the other types type-00_00, 00_01, 00_10, 01_00, 01_10, 10_00, and 10_01 do not. Those types possess the linear characteristics are named linear six-step SWPWM types.

C. Six-Step BEDS

For the sensorless control as shown in Fig. 1, BEDS is used to generate the commutation signal H from the terminal voltages v_a, v_b and v_c. Speed controller tunes the PWM duty ratio *D* according to the speed error between speed command ω_r^* and the estimated speed ω_r where the latter is obtained from calculating the period of commutation signal H. At the same time, all gate signals G_{T1}, G_{T2}, G_{T3}, G_{T4}, G_{T5} and G_{T6} are generated by SWPWM, commutation signal H and PWM duty ratio. The configuration of the comparator-based six-step BEDS for type-01_01 and the illustrated waveforms are plotted in Fig. 4(a) and Fig. 4(b), respectively. As shown in Fig. 4(a), the composition of resistor network and three comparators generates the comparison results H_a, H_b and H_c which are full of PWM transitions.

From Fig. 4(b), we can find that the comparison results H_a, H_b and H_c at floating phase (marked within dashed line) initially keep fixed and then turn to alternate with PWM frequency until the coming back-EMF zero-crossing. Selecting one of the three signals H_a, H_b and H_c obtains the multiplexer signal H_{mux}. Then, a single-trigger function is used to capture the first alternate in H_{mux} after reset action and thus, capture the back-EMF zero-crossing. Finally, delaying the trigger signal H_{trig} by half period $0.5T_{trig}$ yields the adequate commutation signal H where T_{trig} is the period of the trigger signal H_{trig}. The commutation signal H is also feedback to multiplexer to select one position signal at the floating phase.

Due to the conduction of freewheeling diodes at the current commutation, the floating terminal voltage would be equal to V_{dc} or zero until commutation current returns to zero which may result in the failure detection of zero-crossings. Therefore, in order to capture the first edge-change of signal H_{mux} and avoid the conduction effect of freewheeling diodes, a T_d -delayed signal H_{reset} from commutation signal H is used to reset the single-trigger function where the delay time T_d should be set larger than the largest commutation time of free-wheeling diodes in the application.

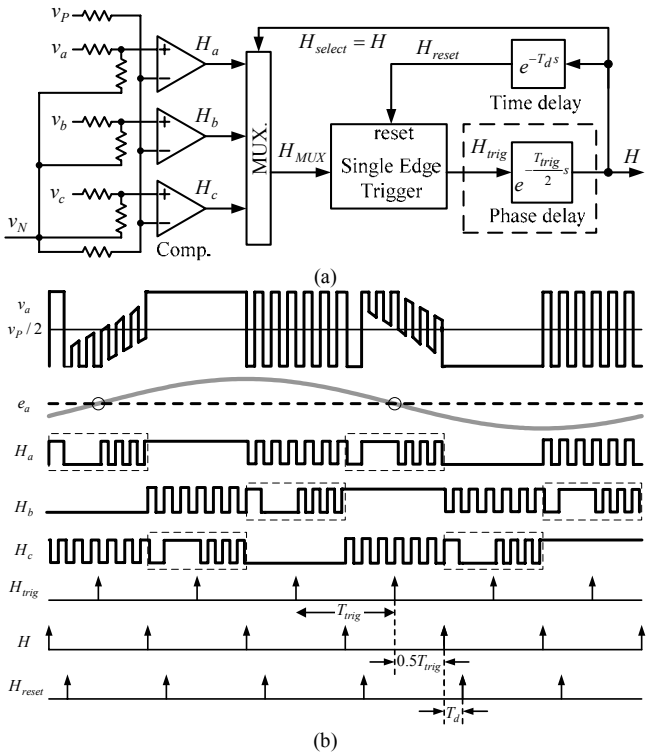

Fig. 4. (a) comparator-based BEDS for type 01_01; and (b) its illustrated waveforms.

D. Sensorless Six-Step SWPWM Types

Obviously, the simple six-step BEDS in Fig. 4 can also be used to obtain the BDCM zero-crossings for other types 01_11, 11_01 and 11_11. Likewise, simple Boolean representation $S_{six-step}$ can be used to represent those sensorless types

$$S_{six-step}=U_2\cdot L_2 \qquad (3)$$

For the six-step SWPWM type-$U_1U_2\_L_1L_2$ as shown in Fig. 2, each floating periods are defined by either combination of U_1 and L_2 or U_2 and L_1. However, from (3), the sensorless types can be easily represented by U_2 and L_2, not the values U_1 and L_1.

In fact, due to the conduction of both freewheeling diodes, the current falling rate with both gate signals "PWM on" is larger than that with only one gate signal "PWM on". It follows that only type-01_01 is used for six-step BEDS [9-10].

III. TWELVE-STEP BEDS

After the development of sensorless six-step SWPWM types and the six-step BEDS, the similar procedure can be applied to find the sensorless twelve-step SWPWM types and develop the twelve-step BEDS in this section.

A. Type Definition for Twelve-Step SWPWM

At any instant, only two switches conduct in the six-step SWPWM. In twelve-step SWPWM, the number of conducting switch changes from two to three, and then changes from three to two. The sequences of conducting devices are $T_1T_2 \rightarrow T_1T_2T_3 \rightarrow T_2T_3 \rightarrow T_2T_3T_4 \rightarrow T_3T_4 \rightarrow T_3T_4T_5 \rightarrow T_4T_5 \rightarrow T_4T_5T_6 \rightarrow T_5T_6 \rightarrow T_5T_6T_1 \rightarrow T_6T_1 \rightarrow T_6T_1T_2$ as shown in Fig. 5. Each switch conducts by $5\pi/6$ and an equivalent $\pi/6$ blanking-time exists between the gate signals at the same leg which avoids the occurrence of short of dc voltage.

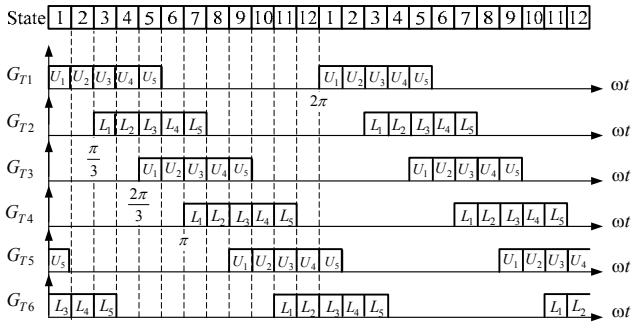

Fig. 5. Type definition of gate signals for twelve-step SWPWM.

It is clear that 150° conduction scheme in each switch is composed of five neighbor conduction patterns. Total ten conduction states are involved in one switch pair. Consequently, it follows that there are $2^{10}=1024$ 150° SWPWM types and each type can be represented as type-$U_1U_2U_3U_4U_5\_L_1L_2L_3L_4L_5$.

Compared to the fixed duty ratio at all states of six-step SWPWM, the twelve-step SWPWM in this paper distributes duty ratio D and reduced duty ratio $(\sqrt{3}/2)D$ at even-number and odd-number states, respectively. It means that the gate signal G_{Tx} may be may be either continuous "on" or discontinuous "on" (i.e. PWM "on") with duty ratio D or discontinuous "on" with reduced duty ratio $(\sqrt{3}/2)D$.

$$G_{Tx}=\begin{cases}\text{Continuous "on"}, & \text{when } U_m=0 \text{ or } L_n=0\\ \text{PWM "on" with duty ratio } D, & \text{when } U_m=1 \text{ or } L_n=1\ (m,n \text{ is even})\\ \text{PWM "on" with duty ratio } (\sqrt{3}/2)D, & \text{when } U_m=1 \text{ or } L_n=1\ (m,n \text{ is odd})\end{cases} \quad (4)$$

For type-00110_00110, two gate signals G_{T1} and G_{T4} of the same leg and the output voltage are plotted in Fig. 6. In order to represent the effect of reduced duty ratio $(\sqrt{3}/2)D$, the output voltage at odd-number patterns (blue waveform) is plotted to a reduced value $(\sqrt{3}/2)V_d$ without change of the average value in each PWM period. In the first $5\pi/6$, we can find that each switch conducts continuously for $\pi/3$, then discontinuously in the following two $\pi/6$ with duty ratios $(\sqrt{3}/2)D$ and D, respectively, and continuously for the remaining $\pi/6$, after this action, the following $7\pi/6$, it blocks.

B. Linear Twelve-Step SWPWM Types

The output voltage $v_{ab}^{150^\circ}$ as shown in Fig. 6 can be expressed in Fourier series as [15]:

$$v_{ab}^{150^\circ}(t)=\sum_{h=1}^{\infty}\frac{16DV_d}{h\pi}\left[\sin\left(\frac{h\pi}{2}\right)\sin\left(\frac{h\pi}{12}\right)\cos\left(\frac{h\pi}{6}\right)\times\cos\frac{(h+1)\pi}{12}\cos\frac{(h-1)\pi}{12}\right]\sin\left(h\left(2\pi f_1 t+\frac{\pi}{3}\right)\right) \quad (5)$$

More zero voltage harmonics can be found in twelve-step SWPWM than six-step SWPWM and consequently, twelve-step SWPWM possesses less voltage distortion than six-step SWPWM. From (2) and (5), we can find $V_{ab,1}^{150^\circ}\geq V_{ab,1}^{120^\circ}$ with a given duty ratio D. However, it is noted that the maximum fundamental voltage $0.989V_d$ of twelve-step SWPWM is smaller than $0.955V_d$ the maximum value of six-step SWPWM. In addition, the maximum fundamental voltage of sinusoidal PWM (SPWM) in linear region is $\sqrt{3}V_d/2\approx 0.866V_d$ which is smaller than the maximum fundamental voltage of six-step and twelve-step SWPWMs.

On the other hand, the fundamental output voltage in twelve-step SWPWM type-00110_00110 can be linearly changed from near zero to its maximum value $0.989V_d$ by adjusting the PWM duty ratio D. However, not all twelve-step SWPWM types possess the same linear characteristics and total 225 linear twelve-step SWPWM types can be found.

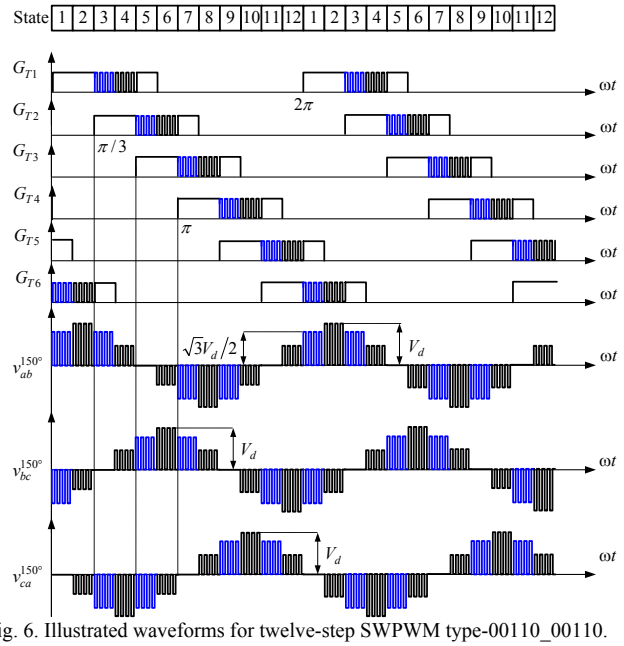

Fig. 6. Illustrated waveforms for twelve-step SWPWM type-00110_00110.

C. Sensorless Twelve-Step SWPWM Types

With the twelve-step SWPWM type-$U_1U_2U_3U_4U_5\_L_1L_2L_3L_4L_5$ shown in Fig. 5, the gate signal changes every $\pi/6$ and the floating periods (i.e. even-number states) are defined by either combination of U_2 and L_4 or U_4 and L_2. Extending (3) yields the Boolean function $S_{twelve-step}$ for sensorless twelve-step SWPWM types

$$S_{twelve-step} = U_4 \cdot L_4 \qquad (6)$$

The gate pattern used in the sensorless control [18] can be seen as twelve-step SWPWM type-10011_10011 and it meets the equation (6) which demonstrates the developed Boolean function $S_{twelve-step}$ in (6) for sensorless twelve-step SWPWM types. In this paper, the twelve-step SWPWM type-00110_00110 with minimum PWM periods is used.

D. Proposed Twelve-Step BEDS

For twelve-step SWPWM type-00110_00110, the resulting comparison waveforms H_a, H_b and H_c are plotted in Fig. 7. Obviously, the zero-crossing signal H_{trig} can be easily separated by an edge-trigger function from H_a, H_b and H_c. In order to obtain the twelve commutation signals from H_{trig}, two auxiliary signals H_1 and H_2 are obtained by delaying signal H_{trig} with time $T_{trig}/4$ and $3T_{rig}/4$, respectively. Then, the commutation signal H is obtained from two auxiliary signals H_1 and H_2.

The proposed twelve-step BEDS is plotted in Fig. 8 where the block in dashed line is the main difference between the six-step BEDS and twelve-step BEDS. Two auxiliary signals H_1 and H_2 are obtained by delaying signal H_{trig} with time $T_{trig}/4$ and $3T_{rig}/4$, respectively. Then, simple OR operation of signals H_1 and H_2 obtains the commutation signal H. A multiplexer is used to select the floating position signal by the signal $H_{select} = H_2$.

Due to the effect of the commutation conduction of freewheeling diodes on the terminal voltage, the reset signal H_{reset} should be a delayed signal from the signal H_2 with T_d to restart the edge-trigger function. Likewise, the BDCM speed ω_r can be estimated from the period of signal H_{trig}.

IV Simulation and Experimental Results

In this section, some simulation and experimental results are provided to evaluate the performances of BDCM sensorless control with six-step SWPWM and twelve-step SWPWM. All the control blocks shown in Fig. 1 and both BEDSs plotted in Fig. 4(a) and Fig. 8 are simulated by PSIM software and implemented in a 16-bit MCU.

A. Simulated Results

With speed command $\omega_r^* = 3000rpm$ and $R_L = 20\Omega$ as shown in Fig. 1, the simulated BDCM currents i_a for six-step SWPWM type-01_01 and twelve-step SWPWM type-00110_00110 are plotted in Fig. 9(a) and Fig. 9(b), respectively, where the sinusoidal-wave back-EMFs e_a is also plotted for comparison. We can find that BDCM sensorless control with both SWPWM types work stably.

Motor current harmonics would result in not only the excess copper loss, but also the torque ripple, the vibration and acoustic noise at the shaft. It follows that less current harmonics is preferred and suitable in motor control. We can find that the total current harmonic distortion (THD_i) value decreases about 20% from 35.11% for six-step SWPWM type-01_01 to 29.34% for twelve-step SWPWM type-00110_00110.

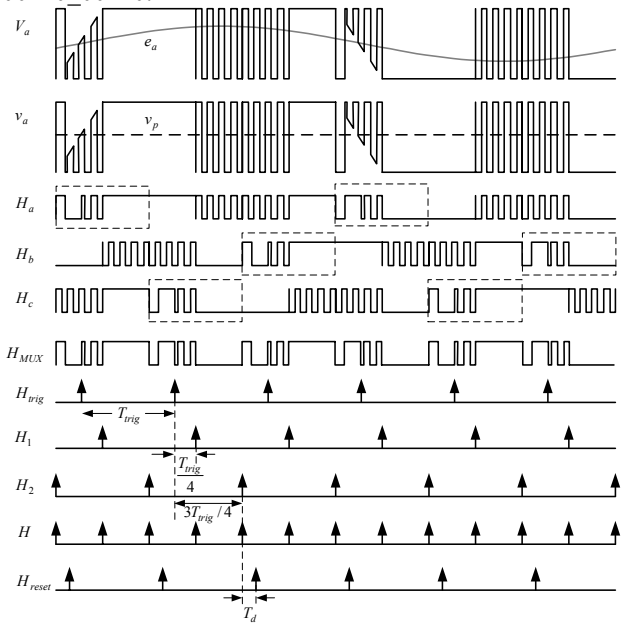

Fig. 7. Illustrated waveforms of the proposed twelve-step BEDS.

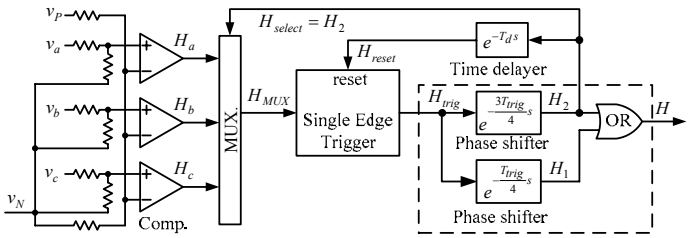

Fig. 8. Proposed twelve-step BEDS.

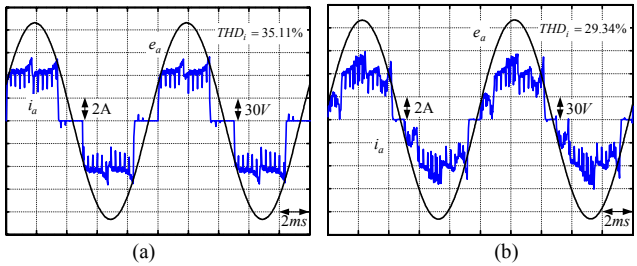

(a) (b)

Fig. 9. Simulated waveforms:(a) six-step SWPWM type 01_01; (b) twelve-step SWPWM type 00110_00110.

B. Experimental Results

As shown in Fig. 1, all sensorless functions including commutation signal generation, speed estimation, speed controller and SWPWM are digitally implemented in MCU. The experimental waveforms for twelve-step SWPWM type-00110_00110 are plotted in Fig. 10. By using the common capture function in general MCU, the signal H_{trig} shows the back-EMF zero-crossings. The commutation signal H is indirectly obtained through two auxiliary signal H_1 and H_2 where signal H_1 and H_2 are also obtained by delaying the trigger signal H_{trig}.

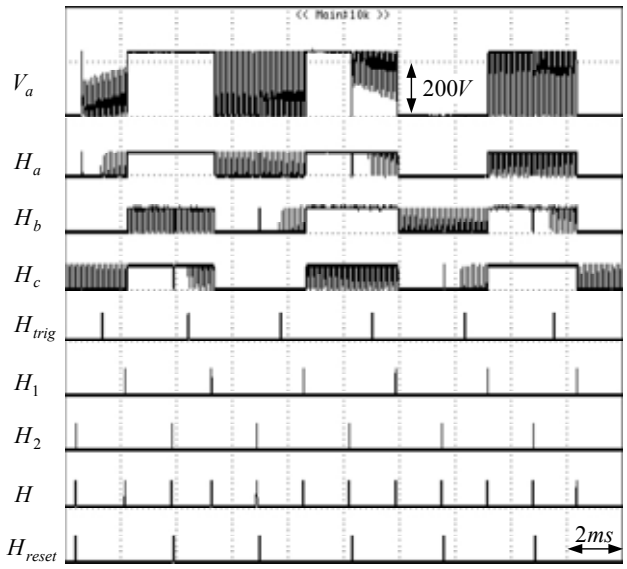

Fig. 10. Experimental waveforms
for twelve-step SWPWM type 00110_00110.

With $R_L = 20\Omega$, the measured gate signals G_{T1} and G_{T4}, position sensing signal H_a and motor winding current i_a at speed $\omega_r = 3000rpm$ for six-step SWPWM and twelve-step SWPWM are plotted in Fig. 11(a) and Fig. 11(b), respectively. The measured THD_i value also decreases from 31.83% to 26.05%. It demonstrates that the proposed BEDS for twelve-step SWPWM work well and can yield less current harmonics than six-step SWPWM.

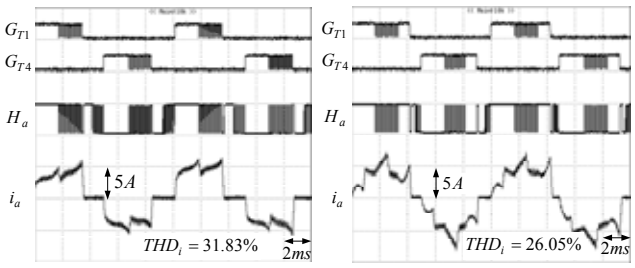

(a) (b)

Fig. 11. Some experimental waveforms (a) for six-step SWPWM type-01_01; (b) for twelve-step SWPWM type-00110_00110.

V. CONCLUSION

Based on the sensorless six-step SWPWM types and six-step BEDS, this paper have studied the twelve-step SWPWM and proposed the twelve-step BEDS. Two auxiliary signals are included in twelve-step BEDS to obtain twelve commutation instants from six back-EMF zero-crossings. The simulated and experimental results also demonstrate the proposed senosorless control with twelve-step BEDS and show about 20% improvement in total current harmonics distortion. The study of linear twelve-step SWPWM types can also contribute to the utilization of twelve-step SWPWM.

REFERENCES

[1] T. Kim, H. W. Lee and M. Ehsani, "Position sensorless brushless DC motor/generator drives: review and furture trends," *IET Proc. Electric Power Applications,* vol. 1, no. 4, pp. 557-564, Jan. 2007.

[2] H. C. Chen, Y. C. Chang, and C. K. Huang, "Practical Sensorless Control for Inverter-Fed BDCM Compressors," *IET Proc. Electric Power Applications,* vol. 1, no. 1, pp. 127-132, Jan. 2007.

[3] Q. Han, N. Samoylenko, and J. Jatskevich, "Average-Value Modeling of Brushless DC Motors with 120 degree Voltage Source Inverter," *IEEE Trans. Energy Convers.,* vol. 23, no. 2, pp. 423-432, June 2008.

[4] H. C. Chen, T. Y. Tsai and C. K. Huang, 'Low-Speed Performance Comparisons of Back-EMF Detection Circuits with Position-Dependent Load Torque,' *IET Proc. Electric Power Applications,* vol. 3, no. 2, pp. 160-169, March 2009. 11-00 BEDS-I

[5] G. J. Su, and W. Mckeever, "Low-Cost Sensorless Control of Brushless DC Motors with Improved Speed Range," *IEEE Trans. Power Electron.,* vol. 19, no. 2, pp. 296-302, March 2004. 11-00 BEDS-I

[6] C. H. Chen, and M. Y. Chen, "Design of a Multispeed Winding for a Brushless DC Motor ant its Sensorless Control," *IEE Proc. Electr. Power Appl.*, vol. 153, no. 6, pp. 834-841, Nov. 2006.

[7] C. C. Wang, G. N. Sung, K. W. Fang and S. L. Tseng, "A low-power sensorless inverter controller of brushless DC motors", in *Proc. of ISCAS'07*, pp. 2435-2438, 2007.

[8] K. H. Kim, and M. J. Youn, "Performance comparison of PWM inverter and variable DC link inverter schemes for high-speed sensorless control of BLDC motor," *Electronics Letters,* vol. 38, no. 21, pp. 1294-1295, 2002.

[9] D. K. Kim, K. W. Lee, and B. I. Kwon, "Commutation Torque Ripple Reduction in a Position Sensorless Brushless DC Motor Drive," *IEEE Trans. Power Electron.,* vol. 21, no. 6, pp. 1762-1768, 2006.

[10] K. W. Lee, D. K. Kim, B. T. Kim, and B. I. Kwon, "A Novel Starting Method of the Surface Permanent-Magnet BLDC Motors without Position Sensor for Reciprocating Compressor" *IEEE Trans. Ind. Appl.,* vol. 44, no. 1, pp. 85-92, 2008. 01-01 BEDS-II

[11] C. T. Lin, C. W. Hung and C. W. Liu, "Position Sensorless Control for Four-Switch Three-Phase Brushless DC Motor Drives," *IEEE Trans. Power Electron.,* vol. 23, no. 1, pp. 438-444, Jan. 2008. BEDS-I

[12] Q. Jiang, C. Bi, and R. Huang, "A New Phase-Delay-Free Method to Detect Back-EMF Zero-Crossing Points for Sensorless Control of Spindle Motors", *IEEE Trans. Magnetics,* vol. 41, no. 7, pp. 2287-2294, July 2005. 00-00 BEDS-I

[13] J. Shao, "An Improved Microcontroller-Based Sensorless Brushless DC (BLDC) Motor Drive for Automotive Applications," *IEEE Trans. Ind. Appl.,* vol. 42, no. 5, pp. 1216-1221, Sep., 2006. 11-00 BEDS-III

[14] Y. S. Lai, and Y. K. Lin, "Novel Back-EMF Detection Technique of Brushless DC Motor Drives for Wide Range Control Without Using Current and Position Sensorls", *IEEE Trans. Power Electron.,* vol. 23, no. 2, pp. 934-940, March 2008. 11-00 BEDS-III

[15] M. H. Saied, M. Z. Mostafa, T. M. Abdel-Moneim, and H. A. Yousef, "On Three-Phase Six-Switch Voltage Source Inverter: A 150-degree Conduction Mode," in *Proc. of ISIE'06*, pp. 1504-1509.

[16] A. Lelkes, J. Krotsch and R. W. De Doncker, "Low-Noise External Rotor BLDC Motor for Fan Applications", in *Proc. of IAS'02*, pp. 2036-2042. 00000-00000 BEDS-I

[17] C. M. Wang, S. J. Wang, S. K. Lin and H. Y. Lin, "A Novel Twelve-Step Sensorless Drive Scheme for a Brushless DC Motor", *IEEE Trans. Magnetics,* vol. 43, no. 6, pp. 2555-2557, June 2007.

[18] S. Saha, Tazawa, T. Iijima, K. Narazaki, H. Murakami and Y. Honda, "A Novel Sensorless Control Drive for an Interior Permanent Magnet Motor", in *Proc. of IECON'01*, pp. 1655-1660. 10011-10011

[19] T. A. Lipo, and D. G. Holmes, "Pulse Width Modulation for Power Converter: Principles and Practice", John Wiley & Sons.